



# Investigation of Swirling Air Flows Generated by Axial Swirlers in a Flame Tube

*Farhad Davoudzadeh*  
*The University of Toledo, Toledo, Ohio*

*Nan-Suey Liu and Jeffrey P. Moder*  
*Glenn Research Center, Cleveland, Ohio*

## NASA STI Program . . . in Profile

Since its founding, NASA has been dedicated to the advancement of aeronautics and space science. The NASA Scientific and Technical Information (STI) program plays a key part in helping NASA maintain this important role.

The NASA STI Program operates under the auspices of the Agency Chief Information Officer. It collects, organizes, provides for archiving, and disseminates NASA's STI. The NASA STI program provides access to the NASA Aeronautics and Space Database and its public interface, the NASA Technical Reports Server, thus providing one of the largest collections of aeronautical and space science STI in the world. Results are published in both non-NASA channels and by NASA in the NASA STI Report Series, which includes the following report types:

- **TECHNICAL PUBLICATION.** Reports of completed research or a major significant phase of research that present the results of NASA programs and include extensive data or theoretical analysis. Includes compilations of significant scientific and technical data and information deemed to be of continuing reference value. NASA counterpart of peer-reviewed formal professional papers but has less stringent limitations on manuscript length and extent of graphic presentations.
- **TECHNICAL MEMORANDUM.** Scientific and technical findings that are preliminary or of specialized interest, e.g., quick release reports, working papers, and bibliographies that contain minimal annotation. Does not contain extensive analysis.
- **CONTRACTOR REPORT.** Scientific and technical findings by NASA-sponsored contractors and grantees.

- **CONFERENCE PUBLICATION.** Collected papers from scientific and technical conferences, symposia, seminars, or other meetings sponsored or cosponsored by NASA.
- **SPECIAL PUBLICATION.** Scientific, technical, or historical information from NASA programs, projects, and missions, often concerned with subjects having substantial public interest.
- **TECHNICAL TRANSLATION.** English-language translations of foreign scientific and technical material pertinent to NASA's mission.

Specialized services also include creating custom thesauri, building customized databases, organizing and publishing research results.

For more information about the NASA STI program, see the following:

- Access the NASA STI program home page at <http://www.sti.nasa.gov>
- E-mail your question via the Internet to [help@sti.nasa.gov](mailto:help@sti.nasa.gov)
- Fax your question to the NASA STI Help Desk at 301-621-0134
- Telephone the NASA STI Help Desk at 301-621-0390
- Write to:  
NASA STI Help Desk  
NASA Center for AeroSpace Information  
7121 Standard Drive  
Hanover, MD 21076-1320



# Investigation of Swirling Air Flows Generated by Axial Swirlers in a Flame Tube

*Farhad Davoudzadeh*  
*The University of Toledo, Toledo, Ohio*

*Nan-Suey Liu and Jeffrey P. Moder*  
*Glenn Research Center, Cleveland, Ohio*

Prepared for  
Turbo Expo 2006  
sponsored by the American Society of Mechanical Engineers  
Barcelona, Spain, May 8–11, 2006

National Aeronautics and  
Space Administration

Glenn Research Center  
Cleveland, Ohio 44135

## Acknowledgments

The NASA Ultra Efficient Engine Technology (UEET) program has supported this work. The authors greatly appreciate the advice, help, and useful suggestions that they received from Ananda Himansu during the course of this research. Furthermore, the authors are grateful to San-Mou Jeng and Jun Cai from the University of Cincinnati for providing the experimental data.

The computer system used was SGI® Altix® 3700 (SGI, Mountain View, CA) superclusters, located at NASA Advanced Supercomputing, NASA Ames Research Center, and the authors appreciate all the help that they received from the NAS personnel during the course of this work.

This report is a formal draft or working paper, intended to solicit comments and ideas from a technical peer group.

This report contains preliminary findings, subject to revision as analysis proceeds.

This report is a preprint of a paper intended for presentation at a conference. Because changes may be made before formal publication, this preprint is made available with the understanding that it will not be cited or reproduced without the permission of the author.

Trade names and trademarks are used in this report for identification only. Their usage does not constitute an official endorsement, either expressed or implied, by the National Aeronautics and Space Administration.

This work was sponsored by the Fundamental Aeronautics Program at the NASA Glenn Research Center.

*Level of Review:* This material has been technically reviewed by technical management.

Available from

NASA Center for Aerospace Information  
7121 Standard Drive  
Hanover, MD 21076-1320

National Technical Information Service  
5285 Port Royal Road  
Springfield, VA 22161

Available electronically at <http://gltrs.grc.nasa.gov>

# INVESTIGATION OF SWIRLING AIR FLOWS GENERATED BY AXIAL SWIRLERS IN A FLAME TUBE

Farhad Davoudzadeh  
The University of Toledo  
Toledo, Ohio 43606

Nan-Suey Liu and Jeffrey P. Moder  
National Aeronautics and Space Administration  
Glenn Research Center  
Cleveland, Ohio 44135

## ABSTRACT

An unstructured and massively parallel Reynolds-Averaged Navier-Stokes (RANS) code is used to simulate 3-D, turbulent, non-reacting, and confined swirling flow field associated with a single-element and a nine-element Lean Direct Injection (LDI) combustor. In addition, the computed results are compared with the Large Eddy Simulation (LES) results and are also validated against the experimental data.

The LDI combustors are a new generation of liquid fuel combustors developed to reduce aircraft NO<sub>x</sub> emission to 70% below the 1996 International Civil Aviation Organization (ICAO) standards and to maintain carbon monoxide and unburned hydrocarbons at their current low levels at low power conditions. The concern in the stratosphere is that NO<sub>x</sub> would react with the ozone and deplete the ozone layer.

This paper investigates the non-reacting aerodynamics characteristics of the flow associated with these new combustors using a RANS computational method.

For the single-element LDI combustor, the experimental model consists of a cylindrical air passage with air swirlers and a converging-diverging venturi section, extending to a confined 50.8-mm square flame tube. The air swirlers have helical, axial vanes with vane angles of 60 degree. The air is highly swirled as it passes through the 60 degree swirlers and enters the flame tube. The nine-element LDI combustor is comprised of 9 elements that are designed to fit within a 76- by 76-mm flame-tube combustor. In the experimental work, the jet-A liquid fuel is supplied through a small diameter fuel injector tube and is atomized as it exits the tip and enters the flame tube. The swirling and mixing of the fuel and air induces recirculation zone that anchors the combustion process, which is maintained as long as a flammable mixture of fuel and air is supplied. It should be noted that in the numerical simulation reported in this paper, only the non-reacting flow is considered.

The numerical model encompasses the whole experimental flow passage, including the flow development sections for the air swirlers, and the flame tube. A low Reynolds number K-ε turbulence model is used to model turbulence. Several RANS calculations are performed to determine the effects of the grid resolution on the flow field. The grid is refined several times until no noticeable change in the computed flow field occurred; the final refined grid is used for the detailed computations. The results presented are for the final refined grid. The final grids are all hexahedron grids containing approximately 861,823 cells for the single-element and 1,567,296 cells for the nine-element configuration.

Fine details of the complex flow structure such as helical-ring vortices, re-circulation zones and vortex cores are well captured by the simulation. Consistent with the non-reacting experimental results, the computation model predicts a major re-circulation zone in the central region, immediately downstream of the fuel nozzle, and a second, recirculation zone in the upstream corner of the combustion chamber. Further, the computed results predict the experimental data with reasonable accuracy.

## INTRODUCTION

Computational fluid dynamics (CFD) has become an integral part in the design process of aer propulsion engines, and a viable tool in understanding complex physical features of flowfields associated with various components of these engines. Use of CFD allows experimentation with new innovative design ideas that was not possible before, due to the excessive cost associated with manufacturing and testing of the prototypes. Thus CFD is able to improve design, reduce development cost, contribute to improved performance, and increase understanding of flowfield induced in not yet fabricated configurations.

In particular, combustion modeling involves many complex physical processes that occur simultaneously such as combustion, turbulence, turbulence chemistry interaction, reaction kinetics, turbulence spray interaction, heat transfer, and radiation. In addition to solving the Reynolds-Averaged Navier-Stokes equations with a turbulence model, one may need to solve tens of individual species mass balance. The required partial differential equations to be solved could easily add up to 30 to 40 equations, depending on the number of species involved in the reaction kinetics. Considering various physical processes that are modeled and the resolution required for the grid to resolve scales of these processes, computational resources needed may become extensive and costly. In addition the complexities of the geometries of the combustors raise the daunting task of curvilinear grid generation.

However, to apply CFD in real-world design applications, the complex 3-D geometries, and many of the physical processes involved need to be resolved. With decreasing computing cost, increasing CPU speed, and the development of the parallel computing platform, computational cost and time is reduced to a level that fit in the design cycle time frame. Furthermore, with the advance of the numerical schemes using unstructured or Chimera meshes, mesh generation is becoming less intimidating than it used to be. The major task still remains the development of schemes and models that address the physics involved and take advantage of the parallel computing.

Ultimately, the proof of validity of any numerical model lies in how well it represents the physics involved in the combustion process within given boundaries and with certain inlet and exit boundary conditions. CFD codes and combustion models developed for gas turbine applications need to be validated against experimental combustor tests with properly characterized inflow conditions, realistic combustion conditions, and detailed velocity and chemical species measurements.

The work described in this paper is a non-reacting RANS simulation of a single-element and a nine-element LDI combustor, and tries to address many of the issues raised above. The combustor modeled here is designed to create a stable, low NO<sub>x</sub> emission flame. The non-reacting experimental velocity data are provided from the experiment for evaluation and validation of the CFD code.

Currently, the simulation is performed for a non-reacting flow. The reacting flow simulation results will be followed in a separate paper.

#### COMPUTATIONAL METHOD:

The computational work performed to produce the numerical results presented in this paper uses the National Combustion Code (NCC), developed at NASA Glenn Research Center (GRC) for comprehensive modeling and simulation of aerospace combustion systems.

The focus in the development of the integrated system of computer codes has been to calculate the fluid, thermal, and chemical characteristics of real-world combustors to an appropriate level of accuracy and turnaround time desired by designers and analysts. The two foremost important obstacles to turnaround time have been grid generation and serial processing.

Use of unstructured or overset grids and parallel computing minimizes the overall time needed to achieve a numerical

solution. Thus the main focus has been to incorporate a numerical scheme that allows use of a large number (thousands) of processors in parallel to shorten the solution time and to provide speed-ups that does not deteriorate with the addition of more processors.

The main flow solver for the code used in this work is based on an explicit four-stage Runge-Kutta scheme, which is very suitable for parallelization. Figure 1 shows an example of the speedup that has been achieved with the code on an SGI Origin 2000 [1]. This 3-D test case uses 1.3 million tetrahedral elements. The parallel speedup metric is calculated by taking the ratio of the time per iteration for the serial case versus the time per iteration for the parallel case. The parallel efficiency is the ratio of the parallel speedup to the number of processors used in the calculation. Davoudzadeh, et.al. [2] reported a factor of two speedup for a 2.5 million elements domain when they increased the number of processors from 200 to 400.

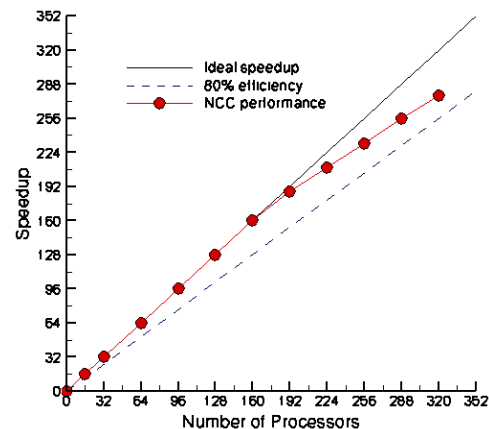


Figure 1. Speedup curve for the 1.3M element test case (Quealy, 2002 [1]).

To facilitate the grid generation task, the code is designed to use unstructured meshes. It uses triangular and/or quadrilateral elements in the 2-D cases, and tetrahedrons, wedges, pyramids, and hexahedrons in the 3-D cases. A combination of these grid types can be used to create hybrid grids. For example, to resolve the boundary layer one may choose to use hexahedron elements in the wall region and transition out of the boundary layer to tetrahedron elements via pyramid elements.

In brief, the flow solver solves steady or unsteady, 3-D, compressible Navier-Stokes equations. The discretization begins by dividing the computational domain into a large number of elements, which can be of mixed types. A central-difference cell-centered finite-volume scheme augmented with numerical dissipation is used to generate the discretized equations, which are then advanced temporally by an explicit 4-stage Runge-Kutta scheme. Low Mach number preconditioning is applied to the governing equations resulting in additional pseudo-time terms. For steady flows, a Runge-Kutta scheme with local stepping in pseudo-time is used as the iterative solution of the governing equations, while unsteady flows use dual-time stepping in which the Runge-Kutta scheme in pseudo-time represents the “inner” iteration. The turbulence model used in the present work is a cubic non-linear k-epsilon model [3] with low Reynolds number wall integration. This

turbulence model is reported [3] to capture the recirculation zones and their structures with more accuracy, relative to the standard k-epsilon model. A description of the solver and some benchmark test cases can be found in Refs. [4-5]. Only steady simulations are reported in the present work.

**EXPERIMENTAL SETUP AND THE GEOMETRY**

The experimental data is provided by Jun Cai, S.-M. Jeng, and R. Tacina [6], and by Yongqiang Fu and San-Mou Jeng [7]. The nine-element fuel injector module is illustrated in Fig. 2a. It comprises an array of 9 injectors that are designed to fit within a 76 mm x 76 mm flame-tube combustor. The center-to-center distance between the elements is 25.4 mm. Figure 2b shows the plane section where the circular flow development sections meet the rectangular cross-section combustion chamber. The single-element configuration is illustrated in Fig. 2c. Each element consists of an air passage with an upstream air swirler and a converging-diverging venturi section. The fuel injector is inserted through the center of swirler and the fuel tip is at the throat of the venturi.

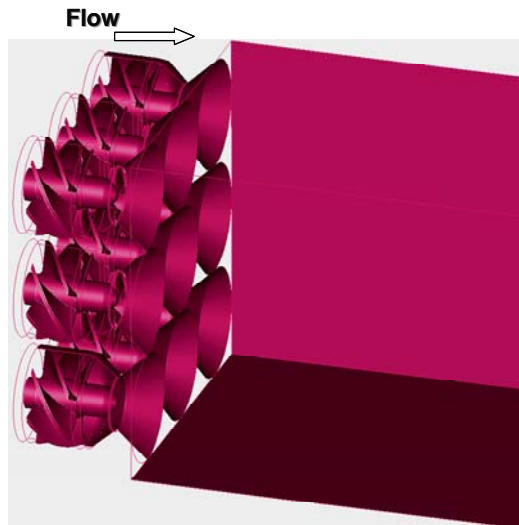


**Figure 2a. Perspective view of the nine-element LDI combustor.**

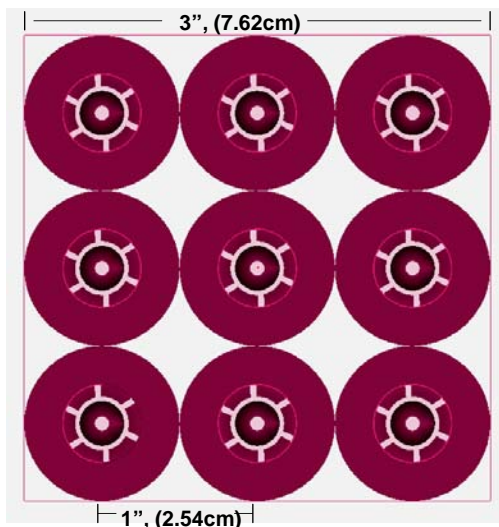


**Figure 2b. Inlet to the combustion chamber.**

Each fuel injector is a simplex type. The fuel injectors are fed by two manifolds so that a limited amount of fuel staging could be evaluated. One circuit feeds the four corner injectors and the center injector, and the second circuit feeds the remaining four injectors (a checkerboard pattern). No Fuel is injected for the non-reacting experiments simulated in the present work.

The air swirlers have helical, axial vanes with downstream vane angles of 60°. There are six vanes with an inside diameter of 9.3 mm and an outside diameter of 22.1 mm. In the array the swirlers are arranged such that each configuration has all the swirlers with the same vane angle. For the current configuration all the swirler vanes have the same sense. The effective area of the air swirler array is 870 mm<sup>2</sup> for the 60° swirlers.

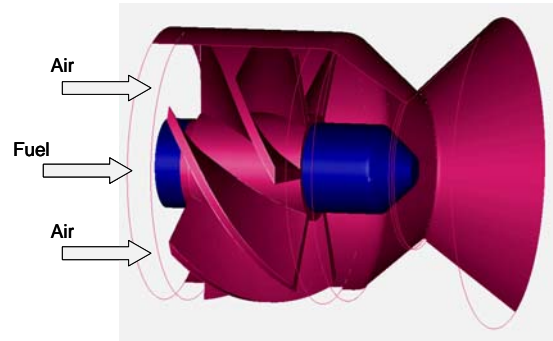


**Figure 2c. Single-element geometry.**

**COMPUTATIONAL DOMAIN AND THE MESH:**

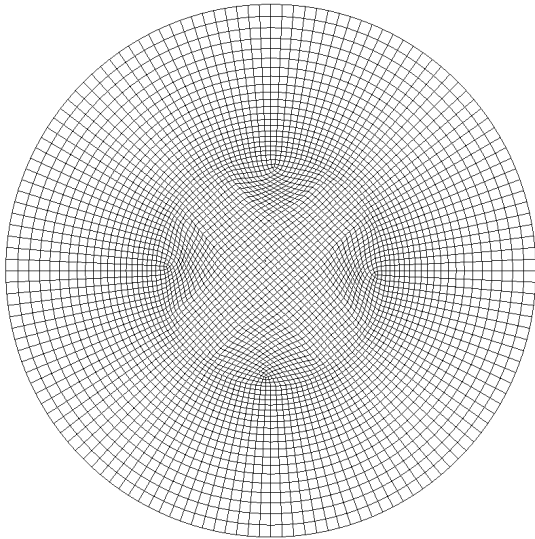
The computational work is performed for non-reacting flow on a single-element combustor and on a nine-element module.

The numerical simulation is performed for the whole geometry including the flow development sections for the air, six swirling air passages for each module and the rectangular section combustion chambers.

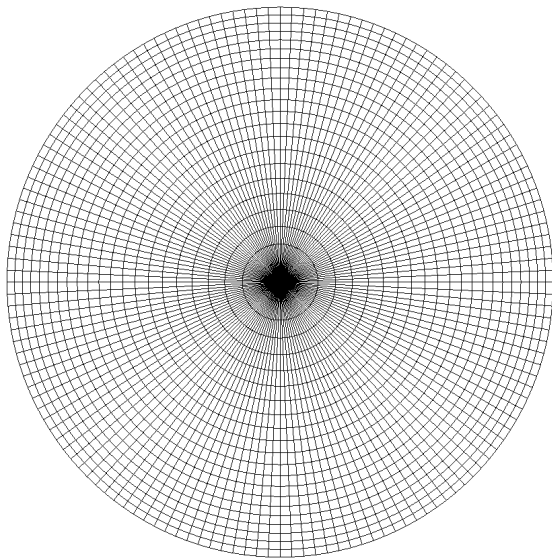
Several grid densities are generated to consider the grid effects. For the single-element geometry three grids with different grid densities namely coarse, medium, and fine are used. The grid densities for the coarse, medium, and fine grids are 240,384 elements, 624,384 elements, and 861,823 elements, respectively. The grids consist of hexahedron-only elements. In contrast to grid topologies where the centerline becomes the axis of singularity around which wedge type elements are generated, in this all-hexahedron mesh, there is no axis of singularity (see Figure 3).

Since the computational code allows for unstructured elements, the hexahedron elements can be constructed in any arbitrary arrangements relative to each other. This allows some degrees of freedom for creating the grid which in turn accelerates the grid generation process. The grid generation part of the computational work took approximately one week to complete. Although creation of the all-hexahedron grids requires more effort, relative to tetrahedron grids, but it reduces overall number of elements required to achieve the same solution accuracy.

The Gridgen software is used to create all the grids used in the numerical simulation reported in this paper.



- Hex-only Mesh
- No Axis Singularity



- Hex-wedge Mesh
- Axis Singularity

Figure 3. Centerline region grid topologies.

Figures 4 and 5 show the grid distributions used for the single-element calculations and for the nine-element calculations respectively. 1,567,296 cells are used for the nine-element combustor. Figure 6 shows the grid distribution in the inlet of the combustion chamber for the nine-element configuration.

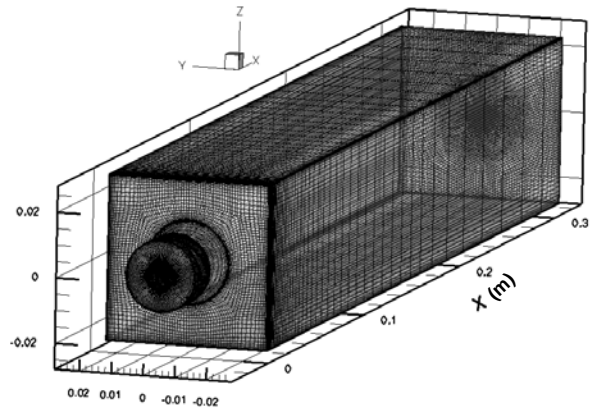


Figure 4. Grid distribution for the single-element LDI combustor.

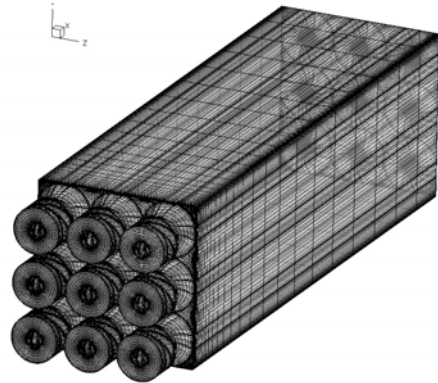


Figure 5. Grid distribution for the nine-element combustor.

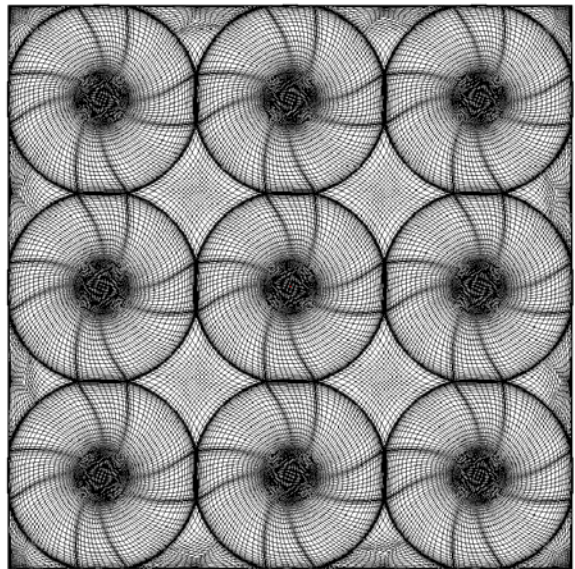


Figure 6. Grid distribution at the inlet of the combustion chamber.

## BOUNDARY CONDITIONS:

The boundary conditions applied for the single module and for the nine element module are different. This was due to the planned experimental work which required two different operating conditions.

**Single-element BC:** Inlet boundary condition specifies the air flow speed (20.14 m/s) normal to the inlet face, density ( $1.19 \text{ Kg/m}^3$ ), turbulence intensity level, turbulence mixing length, and static temperature (294.28 °K.)

**Nine-element BC:** Inlet boundary condition specifies the air flow speed (37.6 m/s) normal to the inlet face, density ( $11.68 \text{ Kg/m}^3$ ), turbulence intensity level, turbulence mixing length, and static temperature (821.98 °K.)

The exit boundary condition for both the single-element and the nine-element specifies static pressure. For the subsonic exit flow, velocity components, enthalpy, turbulent kinetic energy, and dissipation rate are extrapolated from the interior of the domain.

## RESULTS:

The simulation includes the detailed modeling of the entire system--rather than only a passage of the physical domain--including the swirlers' passages. This will eliminate making assumptions for the flow to be necessarily either axisymmetric or periodic. Considering that no detailed experimental data were taken at the inlet of the chamber, alternative approaches, such as eliminating the swirlers and assuming an inlet profile to the combustion chamber, would have introduced more uncertainty to the computation. The inclusion of the swirlers in the computational domain provides an overall more realistic inflow to the main combustion chamber.

Note that, except for the inlet boundary condition, all the experimental measurements were taken inside the combustion chamber, but no experimental data were available to prescribe the inlet to the combustion chamber.

The numerical iteration is carried out until a steady state is reached. The metric for the convergence of the iterations is the residual of the equations being solved. Typically, when the residuals of the momentum equations drop by more than three orders of magnitude, and there is no appreciable change in the solution, the case is considered as converged. The balance of the mass flux into and out of the computational domain is also monitored. When the convergence is reached, the mass balance is also achieved. In considering the above metrics, care should be given to the cases where a local unsteadiness may inhibit the residuals to drop significantly, even though the case may have reached global convergence.

## SINGLE-ELEMENT SIMULATION:

Using the operating conditions described in the boundary condition section, the steady computation is carried out for the single-element and for the nine-element geometries until the residuals dropped by three orders of magnitude. At this time the solution was considered to be globally converged. It should be mentioned that due to the high swirling nature of the flow, some local unsteadiness persevered in the flow field, as will be discussed later.

Figures 7 and 8 show the axial velocity component contours in the X-Z ( $Y = 0.0$ ) and in the X-Y ( $Z = 0.0$ ) planes, respectively. These figures show the presence of a large

recirculation zone in the central core region. The recirculation zone extends upstream up to the face of the injector. These figures indicate that the flow is asymmetric. The red contour levels on the top section of the diverging venturi nozzle on the figure 7 indicate a higher velocity level than the lower part of the nozzle. The pattern is reversed in the X-Y plane shown in figure 8. A more detailed description of the flow structure is revealed in the Fig. 9. In addition to the major recirculation region in the central region, there are two additional regions in which the flow is reversed, one is located immediately aft of the throat when the nozzle is diverging, the other one is located in the corner of the upstream wall of the combustion chamber. The presence and interaction of these vortical structures make the mean flow unsteady in this frontal region. This will become more evident by the high value of the root mean square value of the velocity fluctuations (RMS) in this area measured in the experiments, as will be shown later.

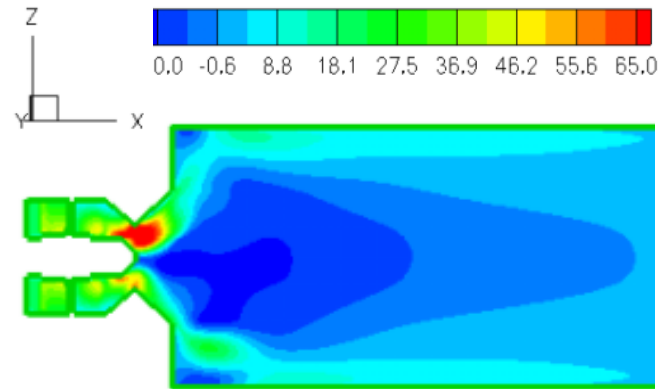


Figure 7. Axial velocity distribution on the  $Y = 0.0$  constant (X-Z) plane.

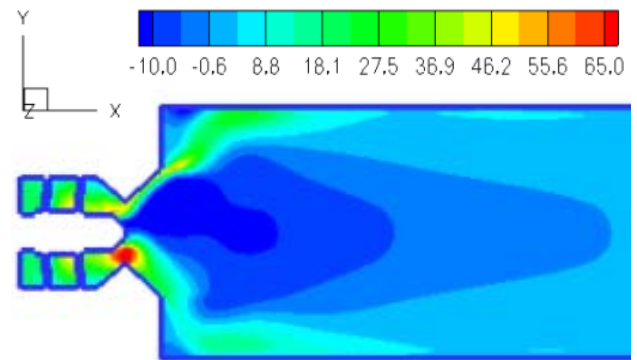
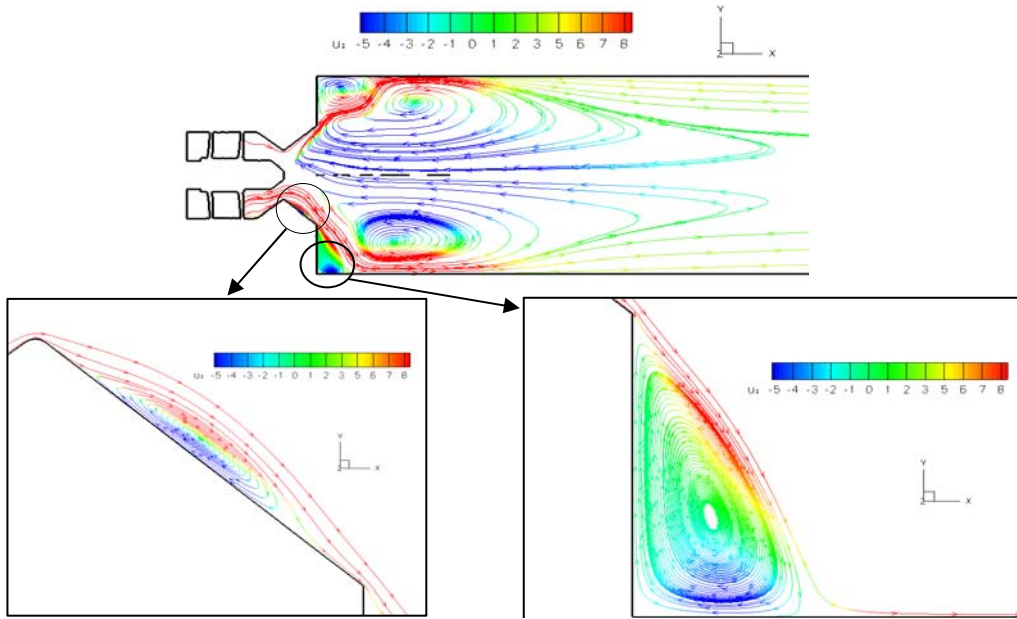


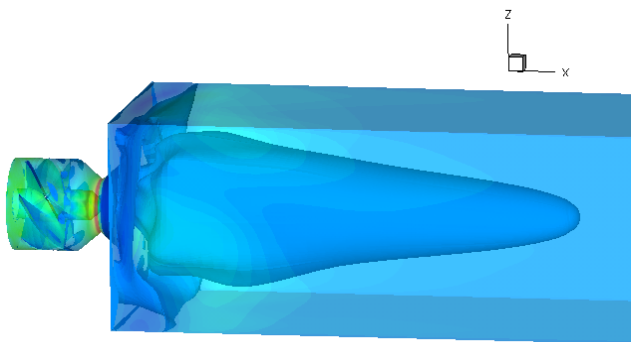
Figure 8. Axial velocity distribution on the  $Z = 0.0$  constant (X-Y) plane.

Fig. 10 shows the perspective view of the iso-surface of zero axial velocity. The iso-surface demonstrates the extent of the central recirculation zone. The corner recirculation zones are also depicted by the zero iso-surface contours. These recirculation zones are located around the root of the large central recirculation zone.



**Figure 9. Particle traces colored by axial velocity, showing the vortical flow structures.**

Figure 11 compares the computed axial velocity with the experimental data, along the centerline of the combustor. The root mean square value of the velocity fluctuations (RMS) from the experimental data is also shown in this figure as vertical bars.



**Figure 10. Iso-surface of zero axial velocity showing the extent of the recirculation zone**

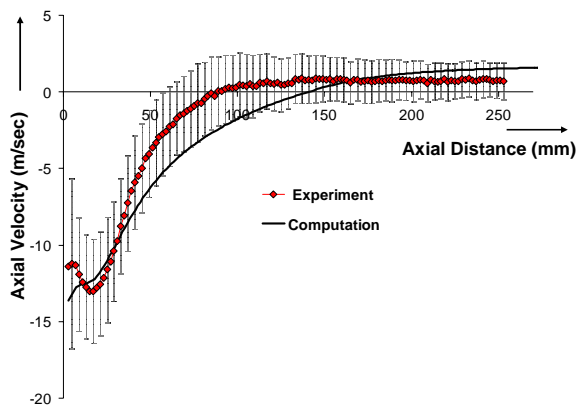


**Figure 11. Computed axial velocity vs. experimental data along the center line.**

The red diamond symbols are the measured values and the solid line is the computed one. The RMS value is high in the inlet of the combustor, indicating the unsteadiness of the flow in this region.

Figures 12, 13, and 14 compare the computed components of the velocity along the y-coordinate, with the measured data for several axial stations. The experimental RMS for the components of the velocity is also shown on some of the curves. The measured RMS value is large for all components of the velocity at the axial station of  $x = 3$  mm. This location is just outside the diverging nozzle and experiences the most unsteadiness in the flow, as indicated by the RMS values. The flow becomes more stable past  $x = 24$  mm, as indicated by the plots. The axial velocity is strong at the inlet across the air-jet. Further, the curves of the axial velocity shown in Fig. 12 indicate that the flow rapidly expands toward the walls, as it enters the combustion chamber. The experimental data demonstrate that the core recirculation zone is somehow thicker than the computed one between the axial stations  $x = 6$  mm to  $x = 12$  mm. However, considering the level of the measured RMS the comparisons are good.

The computed RANS axial velocity profiles at  $x = 3$  mm,  $x = 6$  mm, and  $x = 9$  mm exhibit some asymmetry. This asymmetry can also be noticed in the contour plots shown in figure 9. It should be noted that the dump combustor has a square cross-sectional area, whereas upstream of it, the venturi tube section has a circular cross-section. In other words, the shape of the geometry changes along the flow-passage from periodic six channels to a circular venturi tube, and then a rectangular dump combustor. The anomaly between the geometries of the six upstream blades and the square duct dump combustor is the contributor to this asymmetry in the flow captured by the RANS simulation.

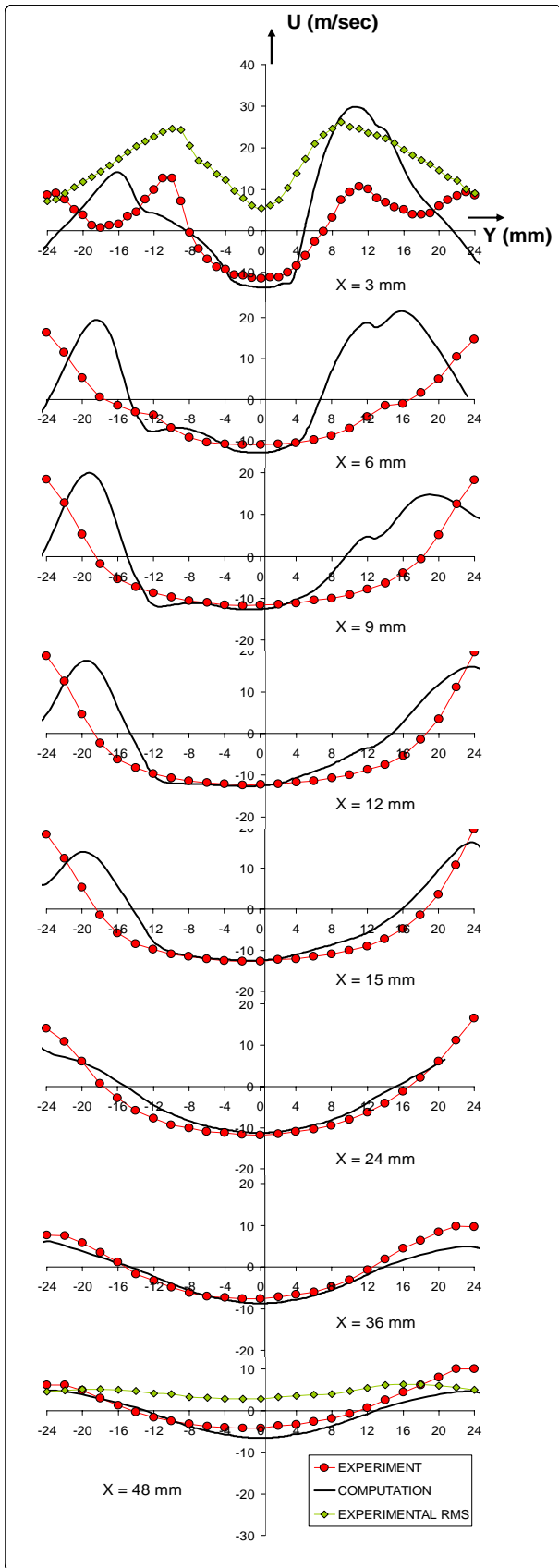


Figure 12. Computed axial velocity (U) at different axial stations compared with the experimental data.

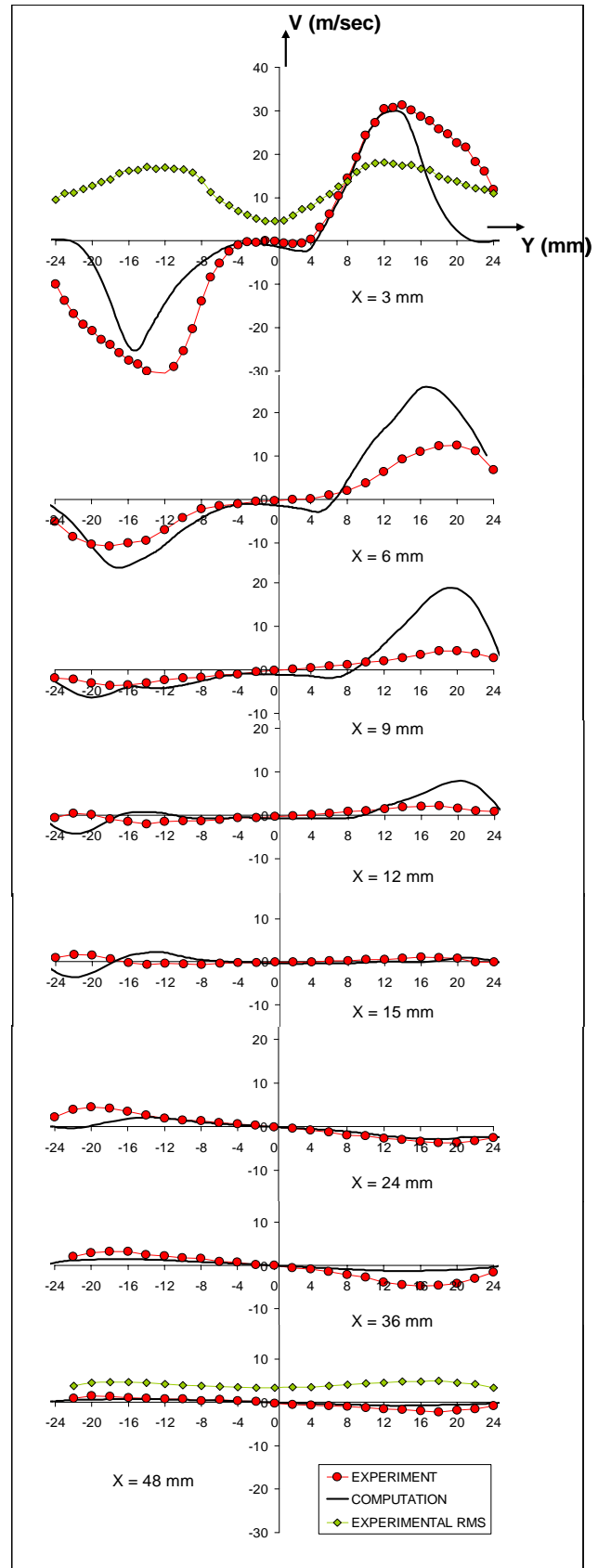


Figure 13. Computed V-velocity at different axial stations compared with the experimental data.

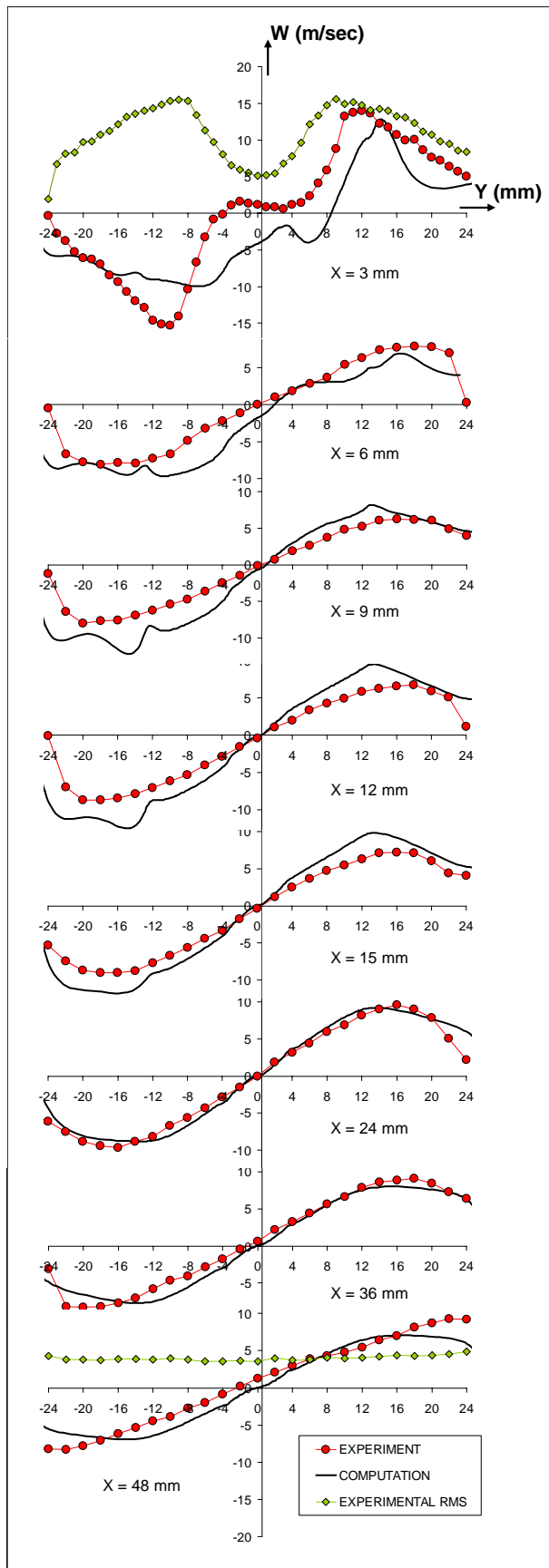


Figure 14. Computed W-velocity at different axial stations compared with the experimental data.

Comparisons for the  $v$ -component of the velocity for the same axial stations and along the  $y$ -coordinate are shown in Fig. 13. It should be noted that at points on the positive part of the  $y$ -axis, the  $v$ -component of the velocity is the same as the radial component of velocity in a polar coordinate system; at points on the negative part of the  $y$ -axis,  $v$ -velocity is the negative of the radial component of velocity. The radial velocity clearly is very high as the flow enters the combustion chamber. Considering the very large central recirculation zone, the flow has to expand toward the wall and move around the recirculation zone. So the radial velocity (or  $v$ -component of the velocity) is very high. Comparing this component of the velocity with the axial velocity, it becomes apparent that the radial velocity at this station (i.e.  $x = 3$  mm) is even higher, in some regions along the  $y$ -axis, than the axial component of the velocity. In the later axial stations, the radial velocity component becomes very small. The radial profile of the axial velocity at station  $x = 3$  mm shows how fast the air jet spreads toward the wall of the combustor.

Figure 14 compares the computed  $w$ -component of velocity with the experimental data along the  $y$ -coordinate for various axial stations. It should also be noted that at points on the positive part of the  $y$ -axis, the  $w$ -component of the velocity is the same as the tangential (swirl) component of velocity in a polar coordinate system; at points on the negative part of the  $y$ -axis,  $w$ -velocity is the negative of the tangential component of velocity. Considering the fact that combustors are designed to create highly swirling flows – for enhanced mixing of the fuel and oxidizer -- this component of velocity is a significant component since it signifies the swirl of the flow. The comparison of the computed results with the measured data for all stations shows the swirl of the flow is computed with a relatively high degree of accuracy. As with other components of the velocity at the first station of  $x = 3$  mm, the experimental data exhibit a locally unsteady flow in this region, as indicated by the measured RMS. Figure 15 shows a better description of this local unsteadiness. It shows the variation of the axial-velocity against the iteration number for several axial points along the center line. It can be noticed that the axial velocity is relatively constant with the iteration number for all axial

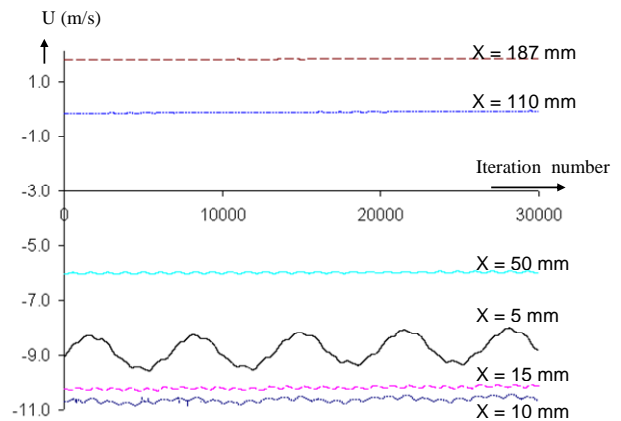


Figure 15. Iteration history of the axial-velocity at various X-Locations along the centerline (iteration No. = 0, corresponds to the restart of the simulation after the global convergence)

stations except  $x = 5$  mm, where periodic oscillations of the velocity about a mean is observed. This is the location where the center core recirculation zone is formed. The vortex in this region is anchored to the injector tip and exhibits some wobbling behavior resulting to the observed axial velocity oscillations in this region.

### THE LES RESULTS:

Through a collaborative work with NASA Glenn, Suresh Menon and his colleagues from Georgia Institute of Technology (GIT) have been conducting Large Eddy Simulations (LES) on the single element LDI described in the previous sections. They have been using the same grid as used in the above RANS calculations. The operating conditions for both RANS and LES have also been the same. Details of their LES method is given in references [8-9]

Considering that the current calculation has been performed by solving steady RANS equations, it would be insightful to compare the results with the LES calculations obtained at GIT.

The LES results presented here are obtained via private communications with Suresh Menon from GIT.

Figures 16, 17, and 18 compare the experimental components of the velocity with the computed RANS results, and with the computed LES results at several axial stations. The velocity components in the LES results are time-averaged mean values.

At  $x = 3$  mm, both RANS and LES results show peak axial velocity away from the centerline which are higher than the measured axial velocity. Furthermore, at this station the measured axial velocity shows emergence of another peak velocity near the wall which is not shown neither by RANS results nor by the LES results.

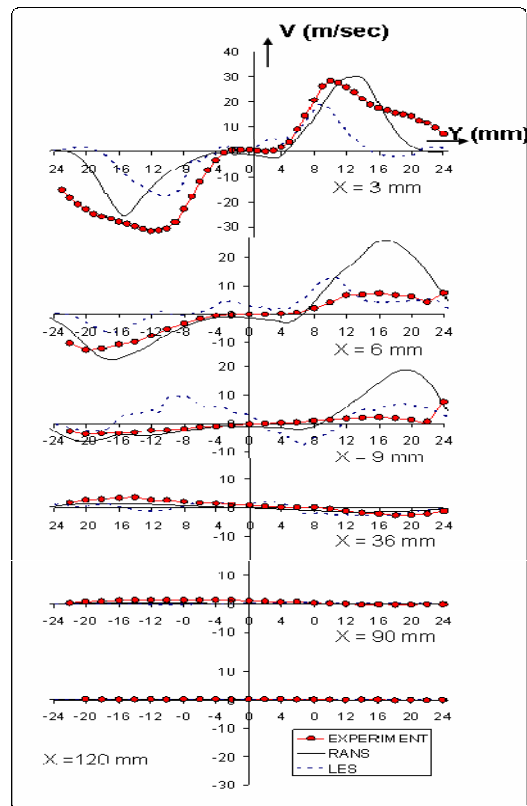


Figure 17. V-velocity profiles at different axial stations for RANS, LES, and the experimental data.

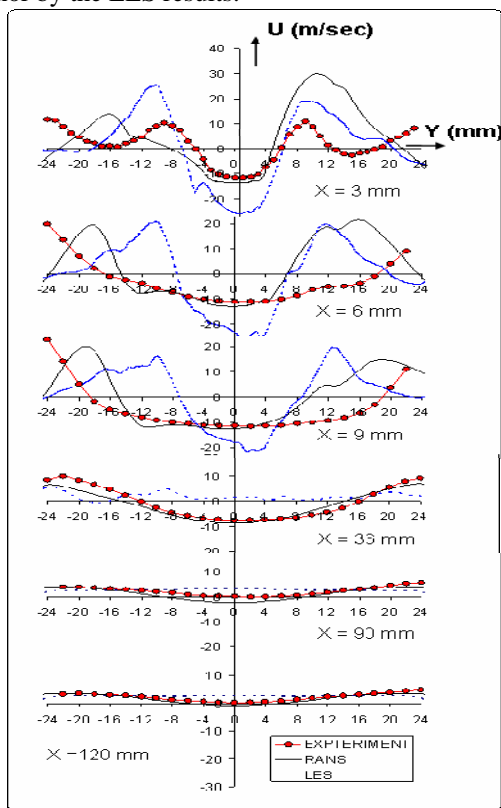


Figure 16. U-velocity profiles at different axial stations for RANS, LES, and the experimental data.

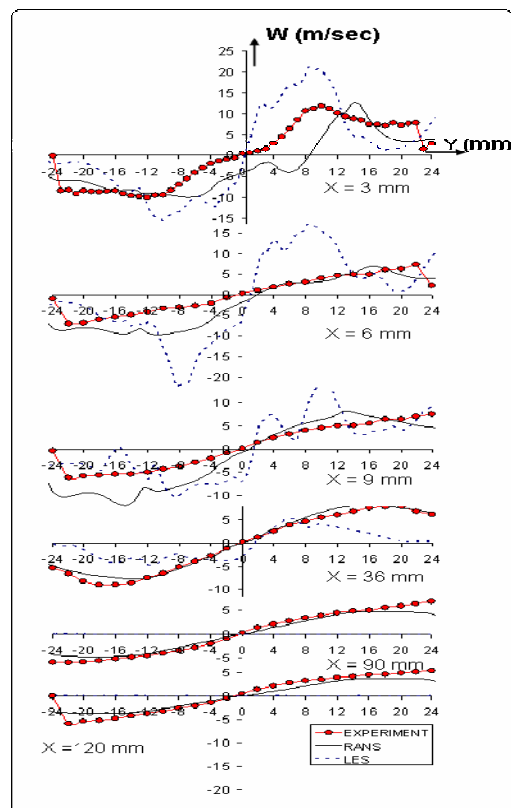


Figure 18. W-velocity profiles at different axial stations for RANS, LES, and the experimental data.

The computed RANS axial velocity profiles at  $x = 3$  mm,  $x = 6$  mm, and  $x = 9$  mm exhibit more asymmetry. This asymmetry can also be noticed in the contour plots shown in figure 9. As mentioned earlier, the dump combustor has a square cross-sectional area, whereas the upstream of it, the venturi tube section has a circular cross-section. In other words, the shape of the geometry changes along the flow-passage from periodic six channels to a circular venturi tube, and then a rectangular dump combustor. The anomaly between the geometries of the six upstream blades and the square duct dump combustor is the contributor to this asymmetry in the flow captured by the RANS simulation.

The axial velocity profiles at  $x = 3$  mm,  $x = 6$  mm, and  $x = 9$  mm given by the RANS results and the experimental data imply a thicker vortex than is predicted by the LES calculations. For these axial stations LES also predicts a stronger reversed flow around the centerline than RANS results or the experimental data. At the axial station  $x = 36$  mm and the stations downstream of it the LES predicts a flat velocity distribution. The RANS results compare well with the experimental data for these axial stations.

Figure 17 shows the v-component of the velocity at the same axial stations for the RANS, the LES, and the experiment.

At  $x = 3$  mm, the RANS results predict the experimental data with more accuracy than the LES results. The LES results also predicts the trend, but underestimates this velocity component for most parts. The predicted flow asymmetry by RNAS, as discussed before, is more pronounced at axial stations  $x = 6$  mm and  $x = 9$  mm. In the further downstream stations the V-velocity profiles are flat.

Figure 18 shows the w-component of the velocity at the same axial stations. As mentioned earlier, at points on the positive part of the y-axis, the w-component of the velocity is the same as the tangential (swirl) component of velocity in a polar coordinate system; at points on the negative part of the y-axis, w-component of the velocity is the negative of the tangential component of velocity. For all stations shown, RANS results predict the experimental data with reasonable accuracy. The LES results over predict the tangential velocity for the  $x = 3$  mm and  $x = 6$  mm. For stations  $x = 36$  mm and  $x = 90$  mm LES tangential velocities are flat.

It should be noted that the current grid used for the computational work is considered to be very coarse for the LES calculations, and this may be partially responsible for the discrepancies observed. Researches at Georgia Institute of Technology are planning to repeat the calculations using a much finer grid.

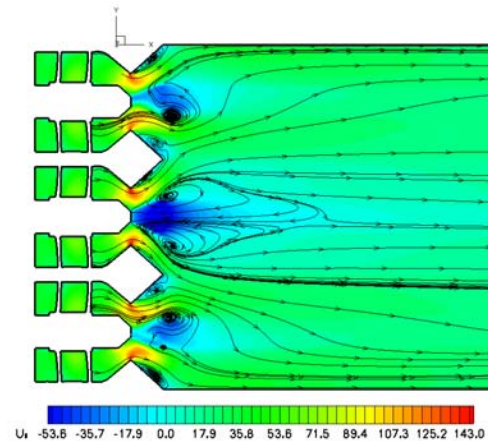
## THE NINE-ELEMENT FLOW SIMULATION

The geometry and the grid for the nine-element configuration are shown in Figs. 2a, 2b, 5, and 6 respectively.

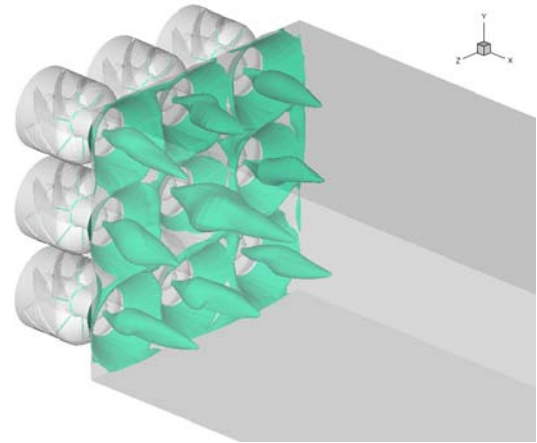
The nine element calculation is performed at the same pressure drop of 4% as for the single-element case. However, the inlet pressure for the nine-element case is set at approximately 27 times the atmospheric pressure with the temperature of 821.98 Kelvin. The boundary condition for the nine element calculation is given in the earlier sections.

Figure 19 shows axial velocity contours on the x-y plane. Particle traces are also shown on this figure. Similar to the single-element calculation there are large recirculation zones downstream of the fuel injectors; in this case nine of them.

These recirculation zones are smaller in their size relative to the single element recirculation zone mainly due to the different operating conditions.



**Figure 19. Axial-section of U-velocity contours and particle traces.**



**Figure 20. Iso-surface of zero axial velocity showing the recirculation zones.**

Figure 20 shows the iso-surface of zero axial velocity indicating all the recirculation zones inside the combustion chamber. A noticeable feature in the flowfield is the extent of the recirculation zone for the center element. This recirculation zone is larger than the recirculation zones created by the surrounding elements. This is due to the fact that unlike the surrounding elements, there is no wall adjacent to the center element, whereas the other recirculation zones are bounded by the side-walls of the combustion chamber.

The axial velocity is high in the air stream for all of the nine elements and the air jet quickly spreads toward the combustor walls. Furthermore, recirculation zones are also formed in the corner regions. All the recirculation zones are well captured by the simulation. These recirculation zones provide a good degree of mixing for the reacting flow and will help to create a stable flame.

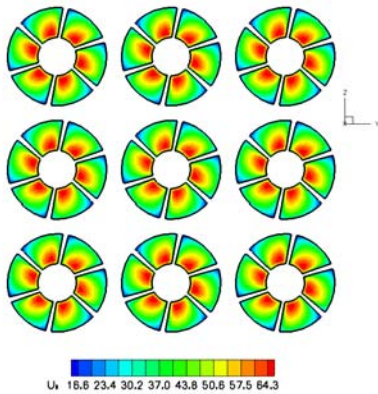


Figure 21a. U-velocity inside the swirler vanes.

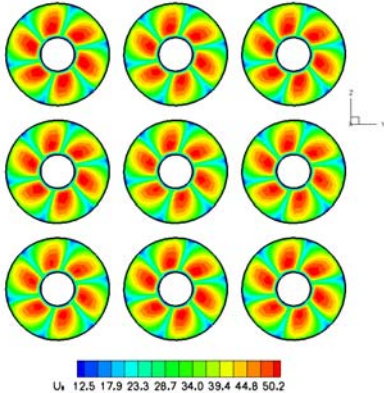


Figure 21b. U-velocity just downstream of the swirler vanes.

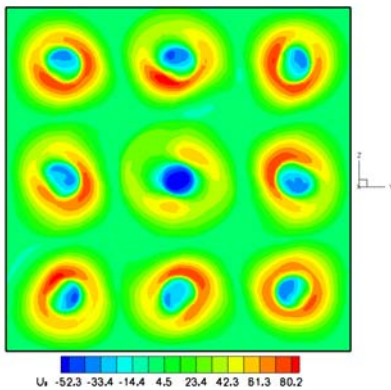


Figure 21c. U-velocity at inlet

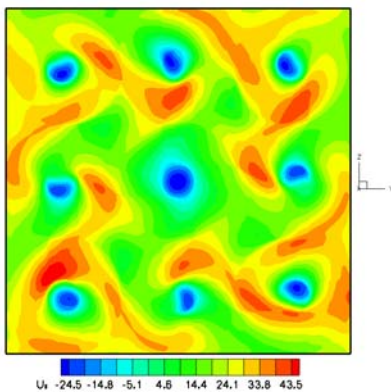


Figure 21d. U-velocity inside the combustion chamber.

Figures 21a-21d show contours of axial velocity inside the swirler vanes, immediately downstream of them, at the inlet to the combustion chamber, and at 6 mm inside the combustion chamber, respectively. Figure 21a is the cross section of the u-velocity, upstream in the swirler region. The white radial lines are the blades. Basically the flow is identical in each passage, since passages are separate and isolated from each other. The only way they can differ from each other would be through the downstream flowfield in the flame tube region. But the downstream effect is not propagating this far upstream. The flow remains similar downstream of the swirler vanes for each element (Fig. 21b). The effects of the combustion chamber recirculation zones become evident at the inlet station to the chamber. As shown in Fig. 21c, there are nine recirculation zones with the center one being stronger than others. At further downstream stations the flow becomes diffused but the influence of the recirculation zones is still evident. The degree of the mixing of the flow is shown in figure 21d which is taken at 6 mm inside the chamber.

Unlike the single-element configuration, there are no aerodynamics experimental data available for comparisons with the computational results. Efforts are underway to produce those experimental data.

### COMPUTATION STATISTICS:

The computer systems that were used to perform the RANS simulations were SGI Altix 3700 Intel Itanium® 2 processors at NAS, NASA Ames Research center. For a non-reacting simulation solving three momentum equations, continuity equation, energy equation, k-epsilon equations, and twelve species equations, the CPU time required per iteration per element is approximately 92 microseconds. Usually it takes about 100,000 iterations to obtain a steady state converged solution. So, using 128 processors and solving for the above equations for a grid consisting of 861,823 elements, it would take approximately 17 hours to obtain a converged solution on the SGI Altix machines. Considering the linear speedup of the code, this time can be reduced to 4.25 hours, if 512 CPUs are used.

### SUMMARY AND CONCLUSIONS:

Any simulation code used for design and analysis of real-world complex flows is required to predict the flow features and the flow quantities with reasonable accuracy and in a reasonable time frame.

An experimental single-element and nine-element LDI combustor exhibiting the typical flow features associated with aircraft combustors is numerically modeled to demonstrate the modeling capabilities of a computer code in predicting the aerodynamics flow characteristics of these combustors.

To minimize the overall turnaround time, unstructured grids are used for the discretization of the partial differential equations and parallel computing system is employed to perform the calculations.

The numerical simulation solves RANS equations together with a cubic non-linear k-epsilon turbulence model.

The simulation is conducted for the full 360° geometry, encompassing 6 air channels for the single-element configuration and 56 air channels for the nine-element configuration.

Results of the simulation demonstrate that the code can predict the essential features of the LDI liquid gas combustors such as the compact re-circulation zone near the tip of the fuel nozzle, and the corner re-circulation zones, with reasonable accuracy. In addition, comparisons of the computed velocity components with the experimental data show good agreements.

The computed RANS results are also compared with the LES results that are obtained from calculations performed on the same geometry and grid, using the same operating conditions. This comparison demonstrated that a much finer grid resolution is needed for the LES calculation of this combustor.

## REFERENCES

[1] Quealy, A., 2002, "National Combustion Code Parallel Performance Enhancements," AIAA Paper No. 2002-3706.

[2] Davoudzadeh, F., and Liu, N.S., : "Numerical Prediction of Non-reacting and Reacting Flow in a Model Gas Turbine Combustor," Proceedings of ASME Turbo Expo 2004, Power for Land, Sea, and Air, June 14-17, 2004, Vienna, Austria.

[3] Shih, T.-H., Chen, K.-H., and Liu, N.-NS., 1998, "A Non-Linear K-epsilon Model for Turbulent Shear Flows," AIAA Paper 98-3983.

[4] Liu, N.-S., "On the Comprehensive Modeling and Simulation of Combustion Systems," AIAA 2001-0805, 39<sup>th</sup> AIAA Aerospace Sciences Meeting & Exhibit, 8-11 January 2001 / Reno, NV.

[5] Ryder, R. C., "The baseline Solver for the National Combustion Code," AIAA Paper 98-3853, July 1998, Cleveland, OH.

[6] Cai, J., S.-M. Jeng, S.-M., "The Structure of a Swirl-Stabilized Reacting Spray Issued from an Axial Swirler," AIAA 2005-1424, 43rd AIAA Aerospace Sciences Meeting & Exhibit, 10-13 January 2005 / Reno, NV.

[7] Fu, Y., Jeng, S.-M., Tacina, R., "Characteristics of the Swirling Flow Generated by an Axial Swirler," Proceedings of GT2005 ASME Turbo Expo 2005: Power for Land, Sea and Air June 6-9, 2005, Reno-Tahoe, Nevada, USA.

[8] Menon, S., Yeung, P. K., and Kim, W. W., 1996. "Effect of subgrid models on the computed interscale energy transfer in isotropic turbulence." *Computers and Fluids*, 25(2), pp. 165-180.

[9] Kim, W. W., Menon, S., Mongia, H. C., 1999. "Large eddy simulation of a gas turbine combustor flow." *Combustion Science and Technology*, 143, pp. 25-62.

**REPORT DOCUMENTATION PAGE**Form Approved  
OMB No. 0704-0188

Public reporting burden for this collection of information is estimated to average 1 hour per response, including the time for reviewing instructions, searching existing data sources, gathering and maintaining the data needed, and completing and reviewing the collection of information. Send comments regarding this burden estimate or any other aspect of this collection of information, including suggestions for reducing this burden, to Washington Headquarters Services, Directorate for Information Operations and Reports, 1215 Jefferson Davis Highway, Suite 1204, Arlington, VA 22202-4302, and to the Office of Management and Budget, Paperwork Reduction Project (0704-0188), Washington, DC 20503.

<b>1. AGENCY USE ONLY (Leave blank)</b>		<b>2. REPORT DATE</b> March 2006	<b>3. REPORT TYPE AND DATES COVERED</b> Technical Memorandum	
<b>4. TITLE AND SUBTITLE</b>  Investigation of Swirling Air Flows Generated by Axial Swirlers in a Flame Tube			<b>5. FUNDING NUMBERS</b>  WBS-516581.02.08.03.05.01	
<b>6. AUTHOR(S)</b>  Farhad Davoudzadeh, Nan-Suey Liu, and Jeffrey P. Moder				
<b>7. PERFORMING ORGANIZATION NAME(S) AND ADDRESS(ES)</b>  National Aeronautics and Space Administration John H. Glenn Research Center at Lewis Field Cleveland, Ohio 44135-3191			<b>8. PERFORMING ORGANIZATION REPORT NUMBER</b>  E-15497	
<b>9. SPONSORING/MONITORING AGENCY NAME(S) AND ADDRESS(ES)</b>  National Aeronautics and Space Administration Washington, DC 20546-0001			<b>10. SPONSORING/MONITORING AGENCY REPORT NUMBER</b>  NASA TM-2006-214252 GT2006-91300	
<b>11. SUPPLEMENTARY NOTES</b>  Prepared for Turbo Expo 2006 sponsored by the American Society of Mechanical Engineers, Barcelona, Spain, May 8-11, 2006. Farhad Davoudzadeh, The University of Toledo, W. Bancroft Street, Toledo, Ohio 43606; Nan-Suey Liu and Jeffrey P. Moder, NASA Glenn Research Center. Responsible person, Farhad Davoudzadeh, organization code RTB, 216-433-8876.				
<b>12a. DISTRIBUTION/AVAILABILITY STATEMENT</b>  Unclassified - Unlimited Subject Category: 01  Available electronically at <a href="http://gltrs.grc.nasa.gov">http://gltrs.grc.nasa.gov</a>  This publication is available from the NASA Center for AeroSpace Information, 301-621-0390.			<b>12b. DISTRIBUTION CODE</b>	
<b>13. ABSTRACT (Maximum 200 words)</b>  An unstructured and massively parallel Reynolds-Averaged Navier-Stokes (RANS) code is used to simulate 3-D, turbulent, nonreacting, and confined swirling flow field associated with a single-element and a nine-element Lean Direct Injection (LDI) combustor. In addition, the computed results are compared with the Large Eddy Simulation (LES) results and are also validated against the experimental data. This paper investigates the nonreacting aerodynamics characteristics of the flow associated with these new combustors using a RANS computational method. The numerical model encompasses the whole experimental flow passage, including the flow development sections for the air swirlers, and the flame tube. A low Reynolds number K-ε turbulence model is used to model turbulence. Several RANS calculations are performed to determine the effects of the grid resolution on the flow field. The grid is refined several times until no noticeable change in the computed flow field occurred; the final refined grid is used for the detailed computations. The results presented are for the final refined grid. The final grids are all hexahedron grids containing approximately 861,823 cells for the single-element and 1,567,296 cells for the nine-element configuration. Fine details of the complex flow structure such as helical-ring vortices, recirculation zones and vortex cores are well captured by the simulation. Consistent with the nonreacting experimental results, the computation model predicts a major recirculation zone in the central region, immediately downstream of the fuel nozzle, and a second, recirculation zone in the upstream corner of the combustion chamber. Further, the computed results predict the experimental data with reasonable accuracy.				
<b>14. SUBJECT TERMS</b> Lean Direct Injection (LDI); Parallel computation; Reynolds-averaged Navier-Stokes (RANS); Unstructured grids			<b>15. NUMBER OF PAGES</b> 18	
			<b>16. PRICE CODE</b>	
<b>17. SECURITY CLASSIFICATION OF REPORT</b> Unclassified	<b>18. SECURITY CLASSIFICATION OF THIS PAGE</b> Unclassified	<b>19. SECURITY CLASSIFICATION OF ABSTRACT</b> Unclassified	<b>20. LIMITATION OF ABSTRACT</b>	



